

Bax-Deficient Mice with Lymphoid Hyperplasia and Male Germ Cell Death

C. Michael Knudson, Kenneth S. K. Tung,
Warren G. Tourtellotte, Gary A. J. Brown, Stanley J. Korsmeyer*

BAX, a heterodimeric partner of BCL2, counters BCL2 and promotes apoptosis in gain-of-function experiments. A *Bax* knockout mouse was generated that proved viable but displayed lineage-specific aberrations in cell death. Thymocytes and B cells in this mouse displayed hyperplasia, and *Bax*-deficient ovaries contained unusual atretic follicles with excess granulosa cells. In contrast, *Bax*-deficient males were infertile as a result of disordered seminiferous tubules with an accumulation of atypical premeiotic germ cells, but no mature haploid sperm. Multinucleated giant cells and dysplastic cells accompanied massive cell death. Thus, the loss of *Bax* results in hyperplasia or hypoplasia, depending on the cellular context.

A family of BCL2-related proteins displays either positive or negative regulatory effects on apoptosis (1). *Bcl2* has the novel oncogenic role of repressing apoptosis and extending cell survival rather than promoting proliferation (2). Membership in the BCL2 family of proteins is principally defined by homology within the BH1 and BH2 domains, which help regulate dimerization (3). This includes BAX (4), which heterodimerizes with BCL2 or BCL_{xL} (5, 6) and when overexpressed counters their protection, promoting cell death. A quantitative analysis within a hematopoietic cell line indicated

that when half or more of endogenous BAX was heterodimerized with either BCL2 or BCL_{xL}, apoptosis was repressed (7).

Given the existence of multiple dimeric partners, the identity of the precise complex that actively regulates the death pathway has remained uncertain. For example, BAX-BAX homodimers might directly activate the death effector pathway, in which case *Bax*^{-/-} mice would be expected to display cellular hyperplasia. Alternatively, if heterodimers of BAX constituted the functionally required repressor complex, then the *Bax* knockout mice could paradoxically display increased apoptosis. BCL2 family members demonstrate some selectivity in their capacity for heterodimerization, but BAX appears to display the greatest capacity for interactions (6, 8). Mice deficient for *Bcl2* (9, 10) or *Bclx* (11) displayed increased apoptosis in selected tissues, which confirms the roles of *Bcl2* and *Bclx* as death repressor molecules.

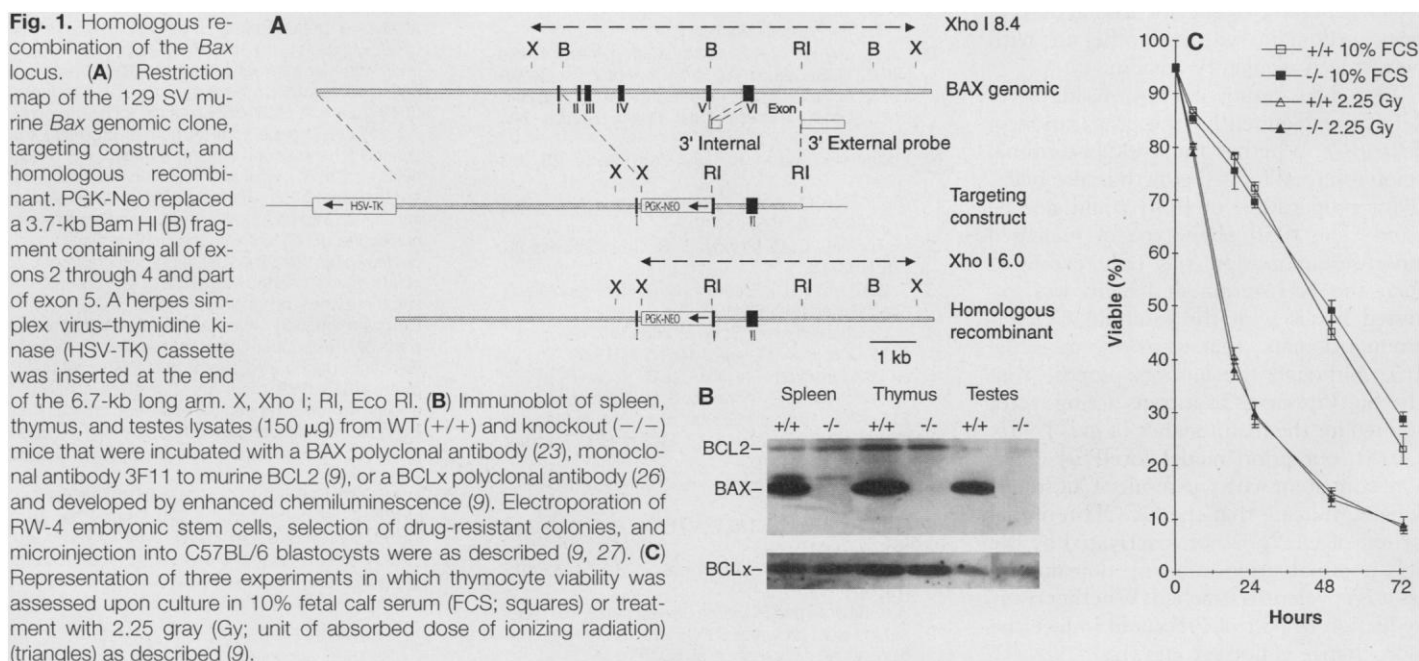
Consequently, we generated a *Bax*-deficient mouse model to address these issues and identify the most critical developmental roles of *Bax*. A *Bax* targeting vector substituted PGK-Neo for exons 2 through 5, deleting BH1 and BH2 and the capacity for a functional protein (Fig. 1A). Two of 89 G418-resistant clones had undergone homologous recombination in RW-4 embryonic stem (ES) cells (12). The disrupted *Bax* allele was ultimately transmitted through the germ line, as confirmed by Southern (DNA) analysis (13). Heterozygous mice appeared normal, and matings resulted in the expected Mendelian frequency of *Bax*^{-/-} mice that grew to adulthood and were externally indistinguishable from wild-type (WT) mice. Immunoblots confirmed the loss of BAX in tissues from *Bax*^{-/-} mice (Fig. 1B). The amounts of the death-repressing molecules BCL2 and BCL_{xL} were comparable in the *Bax*^{-/-} and WT mice.

Although they appeared healthy, *Bax*^{-/-} mice demonstrated selective hyperplasia of lymphoid tissues. Total numbers of thymocytes were 1.6-fold greater in *Bax*^{-/-} mice than in WT controls. However, the percentage of each maturational subset (CD4⁻CD8⁻, CD4⁺CD8⁺, and CD4⁺ or CD8⁺ cells) was not altered. Similarly, spleens in *Bax*^{-/-} mice were enlarged compared to those in WT mice, with greater increases of B cells (1.8-fold) than T cells (Table 1). These B cells had the normal phenotype of mature, resting B cells.

Violation of homeostasis within the lymphoid compartment prompted us to perform assays to assess susceptibility to apoptosis. *Bax*-deficient thymocytes displayed normal viability in serum alone or after treatment with gamma radiation (Fig. 1C) or dexa-

C. M. Knudson, W. G. Tourtellotte, G. A. J. Brown, S. J. Korsmeyer, Howard Hughes Medical Institute and Division of Molecular Oncology, Departments of Medicine and Pathology, Washington University School of Medicine, St. Louis, MO 63110, USA.
K. S. K. Tung, Department of Pathology, University of Virginia Health Sciences Center, Charlottesville, VA 22908, USA.

*To whom correspondence should be addressed.



methasone (13). Thymocyte death induced by gamma radiation depends on p53 (14). p53 up-regulates *Bax* in certain cell deaths (15), prompting the theory that *Bax* may be an effector of p53-induced apoptosis. Our data (Fig. 1C) indicate that *Bax* is not required for p53-dependent apoptosis within thymocytes. Similarly, peripheral T cells had cell death induced by normal activation after treatment with CD3 antibody (13). *Bax*^{-/-} B cells revealed only minimally improved survival after activation with lipopolysaccharide or with immunoglobulin M antibody (13). Thus, these in vitro signals did not appear to fully reproduce the response that leads to the accumulation of *Bax*^{-/-} lymphocytes in vivo.

Male *Bax*^{-/-} mice proved infertile, and adult testes were atrophic (Table 1), with an empty epididymis and vas deferens, indicative of complete cessation of mature sperm cell production. Abnormalities were confined to the seminiferous tubules, none of which can be categorized according to the normal spermatogenic cycle (16) (Figs. 2 and 3). Many tubules exhibited the combination of monotonous cell accumulation,

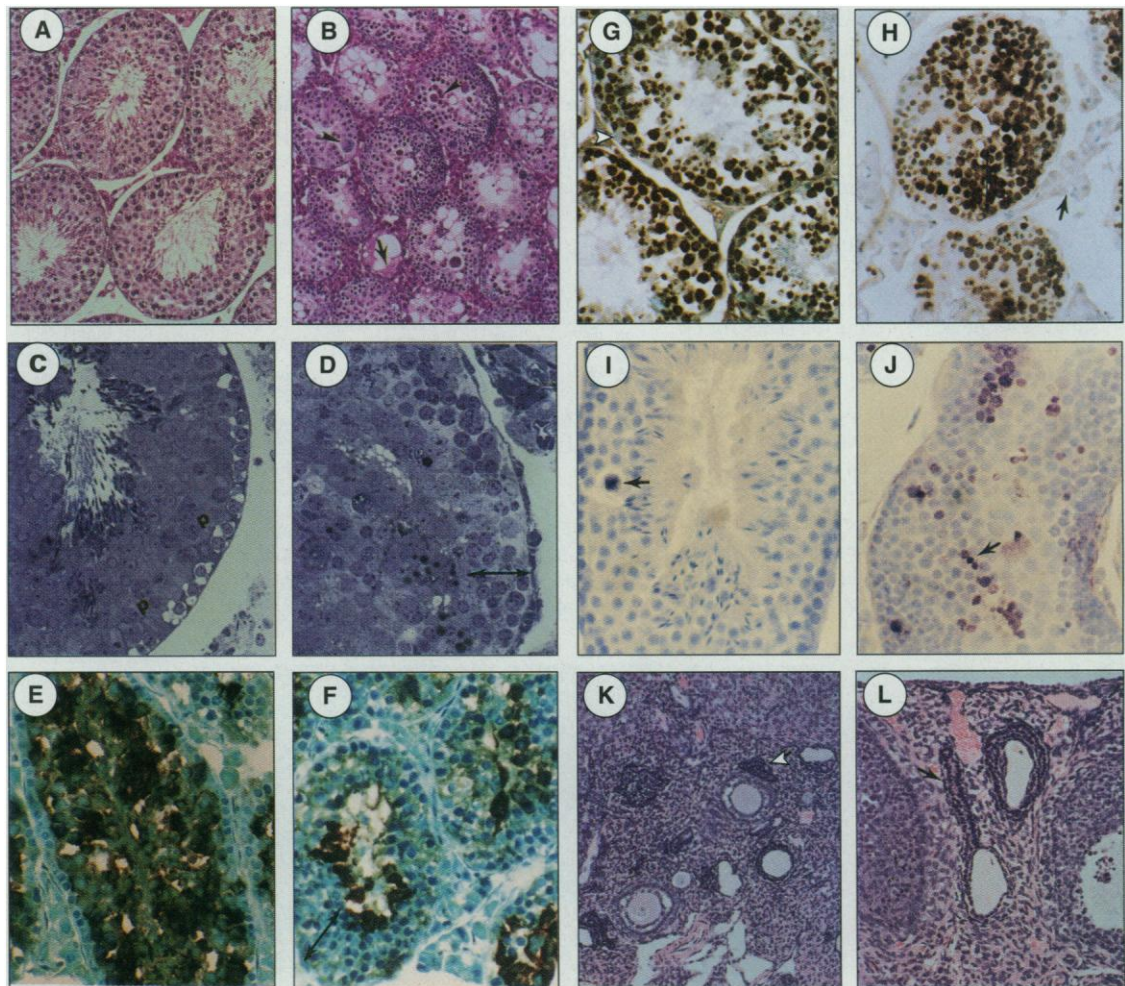
abnormal mitotic or meiotic figures, and multinucleated giant cell formation together with pyknotic cells (Fig. 2, A through D).

The cells that accumulated were situated between the basal lamina and the pachytene spermatocytes, enhancing the

Table 1. Age- and sex-matched WT (+/+) or *Bax*-null (-/-) mature mice were killed, the organs dissected, and the wet weight determined. Thymocyte and splenocyte suspensions were counted and stained with either CD4-phycoerythrin (PE) and CD8-fluorescein isothiocyanate (FITC) or CD3-FITC and B220-PE and analyzed with a FACSCAN flow cytometer. The mean ± standard deviation and the number of mice analyzed (in parentheses) is indicated. Statistical analysis was done with a two independent sample *t* test; two-tailed *P* values are shown when significant (<0.05); NS, not significant.

Characteristic	+/+	-/-	<i>P</i>
<i>Thymus</i>			
Total number (10 ⁶)	99 ± 33 (14)	159 ± 49 (11)	0.002
Weight (mg)	55 ± 16 (10)	75 ± 16.5 (10)	0.014
CD4 ⁺ CD8 ⁺ (%)	78.3 ± 4.1 (14)	77.7 ± 6.6 (14)	NS
CD4 ⁻ CD8 ⁻ (%)	4.5 ± 1.5 (14)	4.1 ± 1.4 (14)	NS
CD8 (%)	3.4 ± 0.7 (14)	3.7 ± 1.1 (14)	NS
CD4 (%)	13.8 ± 2.9 (14)	14.5 ± 4.8 (14)	NS
<i>Spleen</i>			
Total number (10 ⁶)	69 ± 27 (15)	108 ± 34 (11)	0.005
Weight (mg)	98 ± 21 (11)	134 ± 25 (10)	0.003
B220 ⁺ (%)	37.5 ± 5.2 (15)	43.0 ± 6.7 (11)	0.034
CD3 ⁺ (%)	34.2 ± 8.0 (15)	28.2 ± 8.8 (11)	NS
B cells (10 ⁶)	26.1 ± 12.0 (11)	47.5 ± 19.0 (11)	0.005
T cells (10 ⁶)	22.4 ± 11.4 (15)	30 ± 15.8 (11)	NS
<i>Testes</i>			
Weight (mg)	180 ± 22 (4)	98 ± 22 (4)	0.002

Fig. 2. Histology and immunohistochemical staining of *Bax*^{-/-} testis and ovary. (A and B) Hematoxylin- and eosin-stained section of *Bax*^{+/+} (A) and *Bax*^{-/-} testis (B). *Bax*^{-/-} hypocellular tubules (arrow) and multinucleated giant cells (arrowheads) are noted. (C and D) Plastic-embedded sections (1 μm) confirmed the disordered tubule in *Bax*^{-/-} (D) compared to that in +/+ mice (C). An expanded layer of cells has a nuclear morphology characteristic of premeiotic cells (double-headed arrow). The pachytene layer (p) in +/+ testis is noted. (E through H) LDHC4 immunolocalization in *Bax*^{+/+} mice (E) versus that in -/- mice (F) and GCNA1 immunolocalization in *Bax*^{+/+} mice (G) versus that in -/- mice (H) indicates that the expanded cells in -/- testis (double-headed arrows) are premeiotic germ cells. Sertoli cells [arrowhead in (G)] and Leydig cells [arrow in (H)] are negative for GCNA1. (I and J) TUNEL (20) of *Bax*^{+/+} (I) versus that of -/- (J) testes in which labeled cells are denoted by an arrow. (K and L) Numerous atretic follicles with excess residual granulosa cells are present in the ovaries of *Bax*^{-/-} mice [arrow in (K), low magnification]. These atypical atretic follicles, detailed in (L) (arrow, high magnification), are rarely detected in WT mice.



thickness of this cell layer from the normal 1 to 2 layers to 5 to 6 layers (Figs. 2, A through D, and 3). The accumulated cells were in the expected location for spermatogonia and preleptotene spermatocytes (Figs. 2, C and D, and 3). Their nuclear morphology (Fig. 2, C and D), lack of LDHC4 (a marker of pachytene cells and spermatids) (17) (Fig. 2, E and F), and staining for GCNA1 (a nuclear antigen present in spermatogonia through the round spermatid stage) were consistent with this cellular identity (18) (Fig. 2, G and H).

Electron microscopy also documented the disordered maturation scheme (Fig. 3). These premeiotic cells have an atypical distribution of decondensed chromatin and irregular size and shape not typical of spermatogonia or preleptotene spermatocytes (Fig. 3). Of the remaining spermatogenic cells, pachytene cells were reduced in number, round spermatids with PAS (periodic acid-Schiff)-positive acrosomes were rare (13), and elongated spermatids were absent. In a comparison with the extent of cell death known to occur in normal spermatogenesis (19), TUNEL (TDT-mediated dUTP-biotin nick end labeling) (20) identified a marked increase in apoptosis in *Bax*^{-/-} testes with clustered apoptotic germ cells (Fig. 2, I and J). The most severely affected tubules were partially or completely devoid of germ cells (Fig. 2, A and B).

Flow cytometry of cells stained with propidium iodide revealed a marked aberration in the distribution of cells within the *Bax*^{-/-} testes (Fig. 4). A relative increase in 2N cells reflected the abnormal premeiotic cell expansion noted in the testicular sections. Although 4N cells were present, only a small 1N peak representing the round spermatids existed and the more condensed 1N population corresponding to elongated spermatids and spermatozoa was missing. The multinucleated spermatocytes were fragile and not detected by this assay.

Because of such abnormalities, the *Bax*^{-/-} mice represent a genetic aberration in the cell death pathway and provide an unexpected model of male infertility that results in aspermatogenesis. In contrast, the

Bax^{-/-} ovaries displayed relatively normal oocyte development and follicular formation. However, a marked accumulation of unusual atretic follicles contained numerous atrophic granulosa cells that presumably failed to undergo apoptosis (Fig. 2, K and L). This result establishes a role for *Bax* in granulosa cell death, a role also suggested by the responsiveness of *Bax* RNA to ovarian steroids (21).

These knockout mice indicate that *Bax* deficiency can be manifest as hyperplasia or hypoplasia, depending on the cellular context. The widespread expression of *Bax* and its capacity to heterodimerize with multiple family members suggest that it may have a central role in regulating apoptosis. However, the most substantial developmental defects of *Bax* deficiency proved restricted to lineage. Several other family members, *bad* (7) and *bak* (22), also promote cell death and may provide functional redundancy in unaffected lineages. Because the most severe phenotypes in *Bcl2*- and *Bax*-deficient mice involve different lineages, *BCL2* does not appear to function solely through interactions with *BAX*. Individual cell types vary considerably in their composition of *BCL2* family members (23), and elimination of *BAX* would cause different imbalances of dimer pairs. Both positive and negative regulators of apoptosis can be encoded within the same gene (*Bclx_L* and *Bclx_S*) or gene family. The *Bax* knockout indicates that even the same molecule can have a positive or negative effect depending on the cell type.

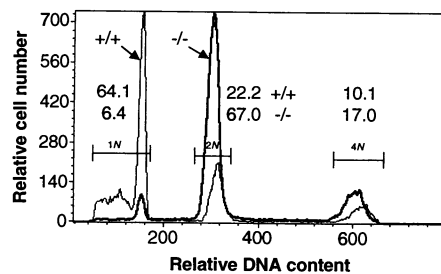
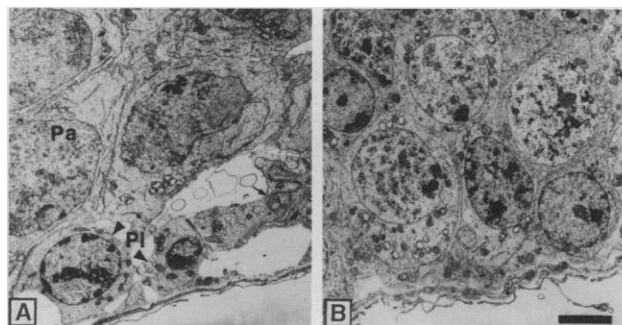


Fig. 4. Flow cytometry histogram of a suspension of testicular cells stained with propidium iodide. Percentage of *Bax*^{+/+} or *Bax*^{-/-} cells in each gate is indicated.

Fig. 3. Electron micrograph of testes. (A) Normal testis with preleptotene spermatocytes (Pl), which are separated from the adluminal compartment by tight junctional complexes between Sertoli cells (arrowhead). Pachytene spermatocytes (Pa) are easily distinguished by their nuclear synaptonemal complexes. (B) *Bax*^{-/-} testis shows the expansion of premeiotic germ cells with an atypical, decondensed (less electron dense), and dispersed chromatin distribution. Size bar, 2.45 μ m.



It is unknown why lymphopoiesis and spermatogenesis are predominantly affected by this mutation. One shared characteristic of lymphopoiesis and spermatogenesis is the need for continuous self-renewal and differentiation programs to generate mature cells. In that respect, spermatogenesis is more affected than oogenesis, and the former requires continued production of gametes in mature testes. A giant cell testicular degeneration syndrome is seen occasionally in p53 knockout mice of certain strains and more dramatically in p53 promoter-CAT (chloramphenicol acetyltransferase) reporter transgenic mice, which have decreased p53 levels in testes (24). The defects in spermatogenesis in both *Bax* and p53 models signify a role for the apoptotic pathway in monitoring male gametogenesis. The massive apoptosis and disorganized spermatogenesis we saw may also indicate a role for *Bax* in regulating the meiotic cycle. The accumulation of atypical premeiotic germ cells may reflect their prolonged survival or a differentiation block that ultimately results in cell death. In other models, overexpression of *Bcl2* or *Bclx_L* has promoted maturation of lymphocytes (25). *Bax*-deficient mice provide evidence for an interrelationship of proliferation, differentiation, and cell death.

REFERENCES AND NOTES

- G. T. Williams and C. A. Smith, *Cell* **74**, 777 (1993); M. Barinaga, *Science* **263**, 754 (1994); C. B. Thompson, *ibid.* **267**, 1456 (1995).
- D. L. Vaux, S. Cory, J. M. Adams, *Nature* **335**, 440 (1988); T. J. McDonnell *et al.*, *Cell* **57**, 79 (1989); D. M. Hockenbery, G. Nunez, C. Millman, R. D. Schreiber, S. J. Korsmeyer, *Nature* **348**, 334 (1990).
- X.-M. Yin, Z. N. Oltvai, S. J. Korsmeyer, *Nature* **369**, 321 (1994).
- Z. N. Oltvai, C. L. Millman, S. J. Korsmeyer, *Cell* **74**, 609 (1993).
- L. H. Boise *et al.*, *ibid.*, p. 597.
- T. W. Sedlak *et al.*, *Proc. Natl. Acad. Sci. U.S.A.* **92**, 7834 (1995).
- E. Yang *et al.*, *Cell* **80**, 285 (1995).
- T. Sato *et al.*, *Proc. Natl. Acad. Sci. U.S.A.* **91**, 9238 (1994).
- D. J. Veis, C. M. Sorenson, J. R. Shutter, S. J. Korsmeyer, *Cell* **75**, 229 (1993).
- K.-i. Nakayama *et al.*, *Science* **261**, 1584 (1993); S. Kamada *et al.*, *Cancer Res.* **55**, 354 (1995).
- N. Motoyama *et al.*, *Science* **267**, 1506 (1995).
- The RW-4 ES cell line was established from strain SV129 by R. L. Wesselschmidt and T. J. Ley.
- S. J. Korsmeyer and C. M. Knudson, data not shown.
- A. R. Clarke *et al.*, *Nature* **362**, 849 (1993); S. W. Lowe, E. M. Schmitt, S. W. Smith, B. A. Osborne, T. Jacks, *ibid.*, p. 847.
- M. Selvakumaran *et al.*, *Oncogene* **9**, 1791 (1994); T. Miyashita *et al.*, *ibid.*, p. 1799; T. Miyashita and J. C. Reed, *Cell* **80**, 293 (1995).
- L. D. Russell, *Am. J. Anat.* **148**, 313 (1977); C. Huckins, *Anat. Rec.* **190**, 905 (1978).
- M. Hintz and E. Goldberg, *Dev. Biol.* **57**, 375 (1977).
- G. C. Enders and J. J. May II, *ibid.* **163**, 331 (1994).
- M. Dym, *Proc. Natl. Acad. Sci. U.S.A.* **91**, 11287 (1994).
- Y. Gaurieli, Y. Sherman, S. A. Ben-Sasson, *J. Cell Biol.* **119**, 493 (1992).
- J. L. Tilly, K. I. Tilly, M. L. Kenton, A. L. Johnson, *Endocrinology* **136**, 232 (1995).
- S. N. Farrow *et al.*, *Nature* **374**, 731 (1995); T. Chit-

- tenden *et al.*, *ibid.*, p. 733; M. C. Kiefer *et al.*, *ibid.*, p. 736.
23. D. M. Hockenbery, M. Zutter, W. Hickey, M. Nahm, S. J. Korsmeyer, *Proc. Natl. Acad. Sci. U.S.A.* **88**, 6961 (1991); D. E. Merry, D. J. Veis, W. F. Hickey, S. J. Korsmeyer, *Development* **120**, 301 (1994); S. Krajewski *et al.*, *Am. J. Pathol.* **145**, 515 (1994); S. Krajewski *et al.*, *ibid.*, p. 1323; M. González-García *et al.*, *Development* **120**, 3033 (1994).
24. V. Rotter *et al.*, *Proc. Natl. Acad. Sci. U.S.A.* **90**, 9075 (1993).
25. G. P. Linette *et al.*, *Immunity* **1**, 197 (1994); D. T. Chao *et al.*, *J. Exp. Med.* **182**, 821 (1995).
26. L. H. Boise *et al.*, *Immunity* **3**, 87 (1995).
27. S. L. Mansour, K. R. Thomas, M. R. Capecchi, *Nature* **336**, 348 (1988).

28. We are indebted to M. Pichler for expert preparation of this manuscript, C. Millman for technical assistance, and J. C. Reed, C. B. Thompson, G. C. Enders, and E. Goldberg for generously providing antibodies. This work was supported by NIH grants CA49712, HD27500, and P30-HD28934.

28 June 1995; accepted 11 September 1995

Dissociation of Synchronization and Excitability in Furosemide Blockade of Epileptiform Activity

Daryl W. Hochman, Scott C. Baraban, James W. M. Owens, Philip A. Schwartzkroin*

Furosemide, a chloride cotransport inhibitor, reversibly blocked synchronized burst discharges in hippocampal slices without reducing the pyramidal cell response to single electrical stimuli. Images of the intrinsic optical signal acquired during these slice experiments indicated that furosemide coincidentally blocked changes in extracellular space. In urethane-anesthetized rats, systemically injected furosemide blocked kainic acid-induced electrical discharges recorded from cortex. These results suggest that (i) neuronal synchronization involved in epileptiform activity can be dissociated from synaptic excitability; (ii) nonsynaptic mechanisms, possibly associated with furosemide-sensitive cell volume regulation, may be critical for synchronization of neuronal activity; and (iii) agents that affect extracellular volume may have clinical utility as antiepileptic drugs.

The two primary features that characterize seizure-associated ("epileptiform") electrical activity in the brain are hyperexcitability and hypersynchronization (1). Although either of these features alone might be sufficient for the development and spread of epileptiform activity, it has not been possible to dissociate them clearly in experimental models of epilepsy. Much basic research on epileptogenesis has focused on synaptic mechanisms underlying changes in excitability (2), but some studies have suggested that nonsynaptic mechanisms might be sufficient to produce hyperexcitability or hypersynchrony. For example, exposing hippocampal slices to Ca^{2+} -free medium abolishes synaptic transmission but produces synchronized burst discharges in the CA1 subfield (3). Investigators have argued that this synchronized activity is mediated by ephaptic interactions among the densely packed CA1 neurons (4). More generally, it has long been supposed that changes in the extracellular space (ECS) could play an important role in modulating normal activity and contributing to pathological levels of excitability or synchronization in the central nervous system (5).

A number of studies have indicated that a major component of ECS volume regulation under normal and pathological conditions is glial dependent (6), and that the furosemide-sensitive Na,K,2Cl cotrans-

porter plays an important role in this function (7). In tissue slices, changes in ECS volume associated with synaptic activity can be monitored by measuring changes in

tissue light-scattering or reflectance (intrinsic optical signal) (8). Stimulus-evoked changes in light transmission through the CA1 region of hippocampal slices are blocked by furosemide (9), but furosemide-treated tissue continues to show normal—or even enhanced—excitatory synaptic responses (9–11). Because the effect of furosemide on the ECS suggests a blockade of nonsynaptic synchronization mechanisms, but its effect on individual neurons suggests an enhancement of synaptic excitability, we performed a series of studies using hippocampal slices to investigate the effects of furosemide on epileptiform discharges. To this end, spontaneous epileptiform activity was elicited by a variety of treatments (12).

In the first of these procedures, episodes of afterdischarges were evoked by electrical stimulation of the Schaffer collaterals (12, 13), and the extracellular field response was monitored in the CA1 pyramidal cell region. The CA1 response to synaptic input was first tested by recording the field potential evoked by a single stimulus pulse. In

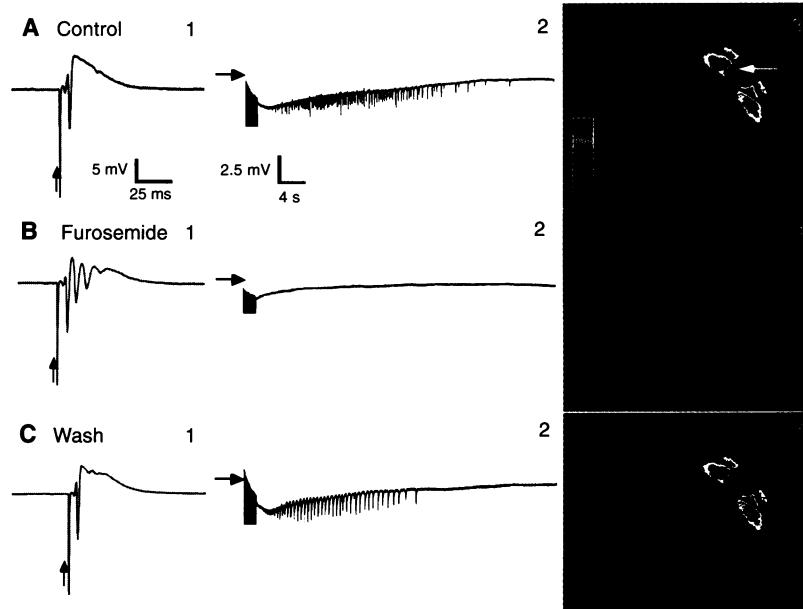


Fig. 1. Effect of furosemide on stimulation-evoked afterdischarge activity. **(A)** Two seconds of stimulation-elicited afterdischarge activity. (A1) The CA1 field response to a single 200- μs test pulse (artifact at arrow) delivered to the Schaffer collaterals. (A2) A typical afterdischarge episode recorded by the extracellular electrode (baseline shown by horizontal arrow). (A3) A map of the peak change in optical transmission through the tissue (reflecting a decrease in extracellular space) evoked by Schaffer collateral stimulation; the region of maximum optical change (red, yellow) corresponds to the apical and basal dendritic regions of CA1 on either side of the stimulating electrode (position indicated by white arrow). **(B)** Responses to stimulation after 20 min of perfusion with medium containing 2.5 mM furosemide. **(C)** Restoration of initial response patterns after 45 min of perfusion with normal bathing medium. For this and the following electrophysiological recordings, negative polarity is downward.

Department of Neurological Surgery, University of Washington, Seattle, WA 98195, USA.

*To whom correspondence should be addressed.